

In situ high-pressure nuclear magnetic resonance crystallography in one and two dimensions ^{EP}

Cite as: Matter Radiat. Extremes **6**, 068402 (2021); <https://doi.org/10.1063/5.0065879>

Submitted: 05 August 2021 • Accepted: 04 October 2021 • Published Online: 21 October 2021

 Thomas Meier, Alena Aslandukova, Florian Trybel, et al.

COLLECTIONS

Paper published as part of the special topic on [High Pressure Science 2021](#)

 This paper was selected as an Editor's Pick



View Online



Export Citation



CrossMark


ARTICLES YOU MAY BE INTERESTED IN

[Everything you always wanted to know about metallic hydrogen but were afraid to ask](#)
Matter and Radiation at Extremes **5**, 038101 (2020); <https://doi.org/10.1063/5.0002104>

[Pressure-induced hydride superconductors above 200 K](#)
Matter and Radiation at Extremes **6**, 068201 (2021); <https://doi.org/10.1063/5.0065287>

[Characterization and performance of the Apollon short-focal-area facility following its commissioning at 1 PW level](#)

Matter and Radiation at Extremes **6**, 064402 (2021); <https://doi.org/10.1063/5.0065138>



Matter and
Radiation at Extremes

Special Issue: High Pressure Science

READ NOW!

In situ high-pressure nuclear magnetic resonance crystallography in one and two dimensions

Cite as: Matter Radiat. Extremes 6, 068402 (2021); doi: 10.1063/5.0065879

Submitted: 5 August 2021 • Accepted: 4 October 2021 •

Published Online: 21 October 2021



View Online



Export Citation



CrossMark

Thomas Meier,^{1,a)}  Alena Aslandukova,² Florian Trybel,³ Dominique Laniel,⁴ Takayuki Ishii,¹ 
Saiana Khandarkhaeva,²  Natalia Dubrovinskaia,⁴  and Leonid Dubrovinsky²

AFFILIATIONS

¹Center for High Pressure Science and Technology Advanced Research, Beijing, China

²Bayerisches Geoinstitut, University of Bayreuth, Bayreuth, Germany

³Department of Physics, Chemistry and Biology (IFM), Linköping University, SE-581 83 Linköping, Sweden

⁴Material Physics and Technology at Extreme Conditions, Laboratory of Crystallography, University of Bayreuth, Bayreuth, Germany

Note: This paper is a part of the Special Topic Collection on High Pressure Science 2021.

a) Author to whom correspondence should be addressed: thomas.meier@hpstar.ac.cn

ABSTRACT

Recent developments in *in situ* nuclear magnetic resonance (NMR) spectroscopy under extreme conditions have led to the observation of a wide variety of physical phenomena that are not accessible with standard high-pressure experimental probes. However, inherent di- or quadrupolar line broadening in diamond anvil cell (DAC)-based NMR experiments often limits detailed investigation of local atomic structures, especially if different phases or local environments coexist. Here, we describe our progress in the development of high-resolution NMR experiments in DACs using one- and two-dimensional homonuclear decoupling experiments at pressures up to the megabar regime. Using this technique, spectral resolutions of the order of 1 ppm and below have been achieved, enabling high-pressure structural analysis. Several examples are presented that demonstrate the wide applicability of this method for extreme conditions research.

© 2021 Author(s). All article content, except where otherwise noted, is licensed under a Creative Commons Attribution (CC BY) license (<http://creativecommons.org/licenses/by/4.0/>). <https://doi.org/10.1063/5.0065879>

I. INTRODUCTION

Nuclear magnetic resonance (NMR) spectroscopy is widely considered one of the most versatile spectroscopic methods available to contemporary natural sciences.¹ Its ability to detect small variations in the nuclear Larmor precession frequency of an $I > 0$ nucleus makes NMR measurements an invaluable tool for electronic and atomic structure determination.²

In contrast to x-ray-based crystallography, probing long-range structural symmetries in solids, quasisolids, and powders,³ NMR crystallography is a well-established method identifying, and often even quantifying, local short-range atomic surroundings or subunits in macromolecules such as proteins.^{4–6}

The application of NMR in extreme conditions research,⁷ in particular at tens of GPa, was widely considered impossible because of the severe technical difficulties in implementing NMR in the devices required for the generation of high pressures, on the one hand, and the inherently low spin sensitivities of polarized nuclear spin ensembles in an external magnetic field, on the other.⁸

Our recent work using magnetic-flux-focusing Lenz lenses has shown that NMR experiments are possible at pressures up to several hundreds of GPa^{9–11} and temperatures above 1000 K.¹² However, this method, although it enables significantly higher pressures to be reached than previous NMR configurations, is generally prone to low spectral resolution, limiting its applicability to the detection of pronounced electronic or magnetic transitions.¹³ Determination of different crystallographic structures, coordination sites, or local environments also remains challenging.

Here, we present our recent progress in developing high-resolution one- and two-dimensional NMR techniques in diamond anvil cells (DACs). This method has been shown to provide intricate structural and electronic insights for a wealth of different systems, namely, diatomic molecules (¹H-NMR on H₂ and ¹⁴N-NMR on N₂), pressure- and temperature-formed metal hydrides (¹H-NMR on YH_x systems), and geophysically important materials [¹H-NMR on (Al_{0.3}, Fe_{0.7})OOH and dense magnesium silicate phase D].

II. STATIC RESONANCE LINE NARROWING TECHNIQUES

The effects leading to significant line broadening in DAC-based NMR studies can be divided into two categories: (1) external line broadening effects such as partial shielding or distortion of the external polarizing magnetic field B_0 by the use of paramagnetic DAC components and (2) nuclear spin interactions inherent to a specific compound. While the former effects can easily be minimized by the use of different materials, suppression of the latter proves to be difficult.

The dominant nuclear spin interactions leading to resonance frequency dispersion are interactions due to homo- or heteronuclear dipole–dipole interactions (\mathcal{H}_{DD}), coupling of the quadrupole moment of $I > 1/2$ nuclei with the surrounding electric field gradient of the charge symmetry (\mathcal{H}_Q), interaction with paramagnetic centers (\mathcal{H}_{PM}), and as anisotropies in dia- and paramagnetic shielding tensors ($\mathcal{H}_{CSA,K}$).

To a first-order approximation, analytic expressions for these interactions can be rearranged in a form containing orientation and distance dependences as well as a contribution consisting of information about their respective magnitude $\Xi(I)$:¹⁴

$$\mathcal{H}_i(I, r_{IJ}, \theta) = \frac{3 \cos^2 \theta - 1}{2r_{IJ}^3} \cdot \Xi(I), \quad (1)$$

where the angle θ describes the orientation of the nuclear magnetic dipoles relative to the external magnetic field. Powder averaging over this term leads to characteristic line shapes well known in NMR spectroscopy.¹⁵

Noticeably, all of these spin interactions show a pronounced inverse cubic dependence on atomic distances r_{IJ} . Therefore, the application of pressure often leads to dramatically increased interaction energies as atomic separations are decreased and thus to significantly increased resonance linewidths.

The angular dependence in Eq. (1) has a zero crossing at an angle of 54.7° . Thus, an alignment of all nuclear dipoles toward this so-called magic angle would effectively suppress the most dominant line broadening effects in solids. Two strategies have been developed to accomplish this feat.

In the first of these, mechanical rapid rotation of a sample around the magic angle, so-called magic angle spinning (MAS), is currently the most widely used method in specialized NMR probes for resonance line narrowing, allowing spectral resolutions of the order of 0.1 ppm to be achieved.¹⁶ For efficient line narrowing in MAS, the rotational speed of the sample around the magic angle should be much greater than the dominant spin interaction frequencies. For high-pressure experiments, linewidths of the order of several hundred kHz have repeatedly been reported,^{17–19} far beyond the capabilities of commercially available MAS probes.

In an alternative approach, first introduced by Lee and Goldburg,²⁰ the spin system itself is allowed to precess along the magic angle by the application of a low-amplitude off-resonance pulse (the LG pulse; see Fig. 1). Signal acquisition is achieved by sampling the zero-time free induction decay intensities in the laboratory frame for different time increments of the LG pulse. The resulting free induction decay in the rotating frame (FIDRF) will be dependent solely on those spin interactions that are linear in the nuclear Zeeman interaction, such as isotropic chemical, paramagnetic, or Knight shifts.

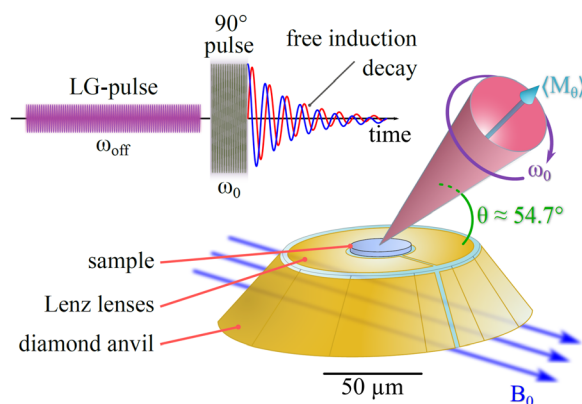


FIG. 1. Schematic representation of Lee–Goldburg decoupling pulse experiments in DACs. By irradiating the sample with a long and weak off-resonance pulse, the precessing spin system is forced to relax in the magic angle $\Theta \approx 54.7^\circ$ (see the text for details), effectively averaging out dominant nonsecular spin interactions. The resulting free induction decay in the rotating frame (FIDRF) will be subject only to those spin interactions that are linear in the nuclear Zeeman interaction perturbation (e.g., isotropic chemical, paramagnetic, or Knight shifts).

While this approach has the advantage that it can be conducted using NMR equipment without rapid mechanical rotation (i.e., static equipment), the necessary radio-frequency field amplitudes and bandwidths of standard probes often limit its effectiveness. However, high-pressure NMR setups are usually equipped with rather small resonators—and thus large radio-frequency field amplitudes—capable of sustaining large bandwidths.²¹

In an LG-NMR experiment, an effective radio-frequency magnetic field \vec{B}_{eff} will be generated by the NMR coil:

$$\vec{B}_{eff} = \left(B_0 - \frac{\omega_{off}}{\gamma_n} \right) \cdot \vec{k} + B_1 \cdot \vec{j}, \quad (2)$$

where B_0 is the external magnetic field amplitude, ω_{off} is the off-resonance frequency of the LG pulse, γ_n is the gyromagnetic ratio of the NMR probe nucleus, and B_1 is the amplitude of the radio-frequency field of the NMR coil. \vec{k} and \vec{j} are unit vectors along the directions of B_0 and B_1 , respectively. The most general expression for B_1 generated by solenoidal coils is

$$B_1 = \sqrt{\frac{\mu_0 Q P_{pulse}}{2\omega_0 V_{coil}}}, \quad (3)$$

where μ_0 is the vacuum permeability, $Q = \omega_0 L/R$ is the quality factor of the resonant circuit (where ω_0 is the nuclear Larmor frequency, L is the inductance, and R is the AC resistance of the tank circuit), P_{pulse} is the average pulse power, and V_{coil} can be approximated by the inner volume of the coil.

The angular dependence in Eq. (1) is zero for $\theta = \arccos(1/\sqrt{3}) \approx 54.7^\circ$, and thus the angle between \vec{B}_{eff} and \vec{B}_0 , using Eq. (2), becomes

$$\tan \theta = \sqrt{2} = \frac{B_1}{B_0 - \omega_{off}/\gamma_n}. \quad (4)$$

Therefore, using the resonance condition for NMR, $\omega_0 = \gamma_n B_0$, the frequency offset $\Delta\omega$ in rad/s of the LG pulse relative to the spectrometer frequency can be obtained as

$$\Delta\omega = \omega_0 - \omega_{\text{off}} = \frac{\gamma_n B_1}{\sqrt{2}}. \quad (5)$$

For *in situ* NMR in DACs using Lenz-lens-based radio-frequency spin excitation, the amplitude B_1 of the driving Helmholtz coil arrangements is typically of the order of 1 mT, leading to offset frequencies of about 30 kHz at $B_0 = 7.04$ T, which are well within the capabilities of high-pressure NMR probes. Therefore, LG-based homonuclear spin decoupling experiments appear as a natural, and very powerful, tool for high-pressure NMR experiments where high spectral resolutions are necessary.²²

III. EXPERIMENTAL

The DACs for high-pressure NMR experiments were prepared following a procedure close to the typical one. First, rhenium gaskets were indented to the desired thickness, which depends on the size of the diamond anvil culets employed, but is usually not more than 25 μm . Sample cavities were drilled using specialized laser drilling equipment. After gasket preparation, the diamond anvils were covered with a layer of 1 μm of copper or gold using chemical vapor deposition. To ensure electrical insulation of the conductive layers from the rhenium gasket, the latter was coated with a thin layer (≈ 500 nm) of Al_2O_3 using physical vapor deposition. The Lenz lens resonators were shaped from the conductive layer on the diamonds using focused ion beam milling.

Before the final cell assembly, radio-frequency resonators were prepared according to their desired operation frequency. A pair of high-inductance solenoid coils (≈ 100 nH) for low-frequency experiments at below 100 MHz or a pair of single-turn printed circuit board (PCB)-plated copper resonators for ^1H -NMR frequencies at high fields (e.g., 300 MHz) were used as driving coil arrangements for the Lenz lens resonator structure and were placed around each diamond anvil, as shown in Fig. 2. After sample loading and initial pressurization, the driving coils were connected to form a Helmholtz-coil-like arrangement.

Pressure calibration was performed using the shift of the first derivative of the first-order Raman signal of the diamond edge in the

center of the culet.^{23,24} All DACs were fixed and connected to home-built NMR probes equipped with customized cylindrical trimmer capacitors (dynamic range ≈ 150 pF) for frequency tuning to the desired resonance frequencies and impedance matching to the spectrometer electronics (50 Ω). All experiments were conducted at a magnetic field of 7.04 T, corresponding to a ^1H frequency of 300 MHz.

Proton shift referencing was conducted using the ^{63}Cu resonances of the Lenz lenses themselves as internal references, taking into account the additional shielding of B_0 inherent to every DAC. These resonances were cross-referenced with standard metallic copper samples under ambient conditions without a DAC. The resulting shift between the two ^{63}Cu -NMR signals was then used as a primer for the NMR signals of the samples under investigation.

LG decoupling experiments were initially calibrated by rapid 2D nutations (about 56 2D spectra) for different off-resonant frequencies of the LG pulse. Optimal ω_{off} values were found to be between 25 and 35 kHz, in agreement with our calculations [Eq. (5)]. 1D LG spectra were recorded by oversampling in the indirect time domain (about 8000 increments) using previously determined values of ω_{off} at a 10 dB pulse power attenuation relative to the excitation pulse. 2D LG spectra were recorded with identical direct and indirect time domains (usually 2048 points in each dimension), while matching the incrementation of the LG pulse to the direct time-domain dwell time of the spectrometer. This procedure ensures correct scaling of the indirect LG frequency domain after 2D Fourier transformation.²⁵

IV. PERFORMANCE OF LG DECOUPLING WITH LENZ-LENS-BASED NMR RESONATORS

To demonstrate the advantages of LG decoupling in DAC-based NMR experiments, we compared the LG performance between a standard solenoidal microcoil (500 μm diameter, 750 μm height) and Lenz-lens-based NMR resonators. Ideal LG conditions were determined in both cases.

First, we performed 1D ^{19}F -LG-NMR experiments on a single crystal of CaF_2 by incrementing the saturation pulse in steps of 1 μs (the maximum length of the LG pulse was 100 μs) at $\Delta\omega \approx 100$ kHz. The zero-time intensity sampling of both real and imaginary parts of the signals [Fig. 3(a)] decay within ~ 125 μs , corresponding to a fivefold stretching of the FIDRF relative to the laboratory frame (FID). The resulting linewidths of the fluorine signals after Fourier transformation could be

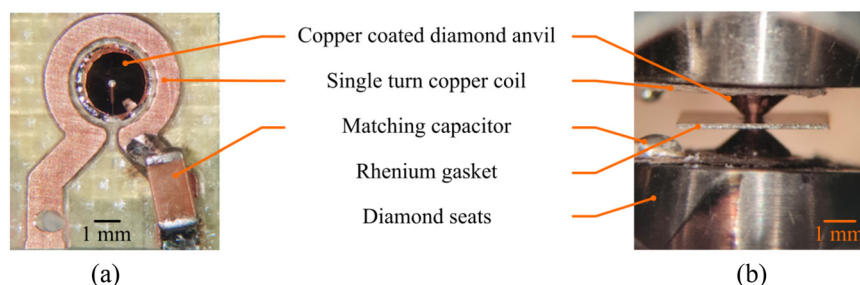


FIG. 2. High-pressure NMR resonator setup for high-frequency applications. (a) To drive the Lenz lens resonators, a pair of single-loop coils made from PCB-plated copper is used. To match the resonators' small inductance (≈ 1 nH) to the desired resonance, a surface-mount device capacitor (≈ 10 nF) is placed in series with each coil. (b) In the closed DAC assembly, a Helmholtz coil arrangement drives the Lenz lens resonators.

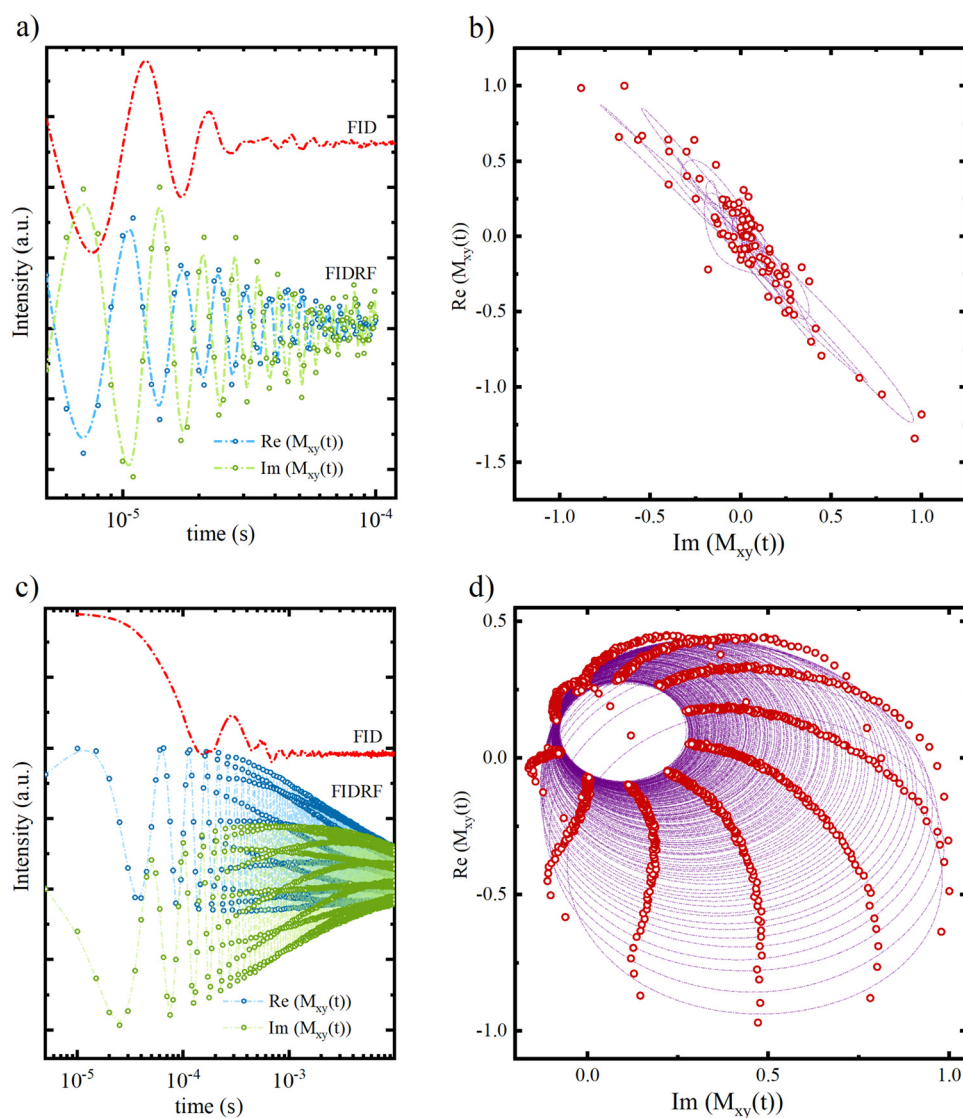


FIG. 3. Comparison of LG decoupling using standard coils and in DACs. (a) ^{19}F -free induction decays in the laboratory frame (FID) and in the rotating frame (FIDRF), sampled as described in the text, of a single crystal of CaF_2 obtained from a 150 pl (500 μm diameter, 750 μm height)-sized solenoidal coil. (b) The corresponding coherence diagram (red dots are data points and the purple lines are guides to the eye) clearly shows a rapid dephasing of the FIDRF within $\sim 100 \mu\text{s}$. (c) ^1H FID and FIDRF of a single crystal of dense magnesium silicate phase D from a Lenz-lens-based resonator design as described in the text. (d) The corresponding coherence diagram shows a slow dephasing of the real and imaginary parts of the FIDRF, corresponding to a stretching factor of about two orders of magnitude. The resulting Fourier transform NMR signal (not shown) has a FWHM linewidth of 0.12 ppm.

reduced from an initial 140 ppm to about 30 ppm. The correlation between real and imaginary parts of the FIDRF [Fig. 3(b)] shows the rapid dephasing of the NMR signal in the rotating frame.

Subsequently, we performed the same experiment on a single crystal of dense magnesium silicate phase D in a DAC at 9 GPa, using LG-pulse increments of $5 \mu\text{s}$ at $\Delta\omega \approx 34 \text{ kHz}$. The resulting FIDRF [Fig. 3(c)] exhibits a very slow decay of signal amplitudes. Data acquisition in the indirect LG time domain was cut off before complete signal decay was achieved, owing to spectrometer

limitations. Analysis of the FIDRF indicates a $1/e$ decay constant of about 40 ms. The corresponding coherence diagram [Fig. 3(d)] shows ideal vortex-like behavior of slowly dephasing signal amplitudes. FWHM linewidths of the resulting Fourier transform ^1H -NMR signals were found to be 0.12 ppm.

This comparison demonstrates that homonuclear decoupling in DACs benefits from strong radio-frequency amplitudes B_1 and large excitation and receiving bandwidths of the employed resonator configuration. It is noteworthy that the microcoil used for

experiments on CaF_2 is about four orders of magnitude smaller than regular NMR transceiver coil arrangements, which would lead to even lower B_1 amplitudes and bandwidths.

V. RESULTS

In the following, we give examples of measurements where LG decoupling enables the investigation of

- spin isomerism in molecular hydrogen and nitrogen, which can only be resolved in a 1D analysis owing to the strong decrease in linewidth;
- a subtle spin transition in phase D, via a 2D analysis, which is not resolved in 1D or by other experimental techniques;
- coexisting local chemical environments in δ -(Al, Fe)OOH and different coexisting phases, such as YH_2 and YH_3 , in one experiment, where a 2D analysis leads to a decomposition of the resonances and enables therefore not only an individual analysis, but also a simultaneous analysis at the same pressure and temperature, as well as a quantification of the sample fractions.

A. One dimension

1. ^1H -LG-NMR on molecular hydrogen up to 123 GPa

The results of the first LG decoupling experiments on molecular hydrogen in DACs have been published recently, with spectral resolutions of about 3 ppm being obtained, corresponding to a 1600-fold reduction of the H_2 NMR signals at pressures of up to 123 GPa.¹⁹

Molecular hydrogen is predicted to show a coupling between molecular rotational properties and nuclear spin orientations, giving rise to the spin isomers ortho- and para-hydrogen. We have been able to show that already at $P \geq 70$ GPa, intramolecular nuclear spin

coupling breaks down and the hydrogen spin system adopts an average dipolar $I = 1/2$ value, much lower than the predicted molecular dissociation at the Wigner–Huntington transition.^{26–28} Crossovers of the nuclear spin statistics of quantum solids such as hydrogen have never been observed before, and, given the large compressibility of hydrogen in conjunction with strong nuclear quantum effects, this crossover phenomenon might only be experimentally observable in molecular H_2 .

2. ^{14}N -LG-NMR on molecular nitrogen up to 85 GPa

Similar to molecular diatomic hydrogen, molecular N_2 ^{29,30} and its derived nitrides,^{31–33} stabilized after laser heating under high pressure in a DAC, have attracted great interest in the high-pressure community as high-energy-density materials. Nitrogen-NMR experiments under extreme conditions would be greatly beneficial for investigations of the local electronic and atomic environments of these compounds, but pronounced quadrupolar couplings, low signal intensities, structural complexity, and the necessity for laser-heating-assisted sample synthesis in a DAC under pressure makes nitrogen NMR in DACs extremely challenging.

At natural abundances, the majority of nitrogen molecules will be $^{14}\text{N}_2$ units, with each ^{14}N nucleus possessing integer nuclear spin ($I = 1$). Intramolecular nuclear angular momentum summation leads to the stabilization of two observable nuclear spin isomers: (i) the quintuplet state of spin $I = 2$ ($|I = 2, m_I = \pm 2, \pm 1, 0\rangle$) and (ii) the $I = 1$ spin triplet ($|I = 1, m_I = \pm 1, 0\rangle$), where the singlet state with $I = 0$ is NMR-inactive and not observable. The quadrupolar nature of these spin isomers leads to significantly broadened ^{14}N -NMR spectra of $\geq 10^5$ ppm,³⁴ significantly reducing signal intensities.

Preliminary ^{14}N -NMR experiments on molecular nitrogen at 72 GPa after laser heating to about 2000 K at 130 GPa and room

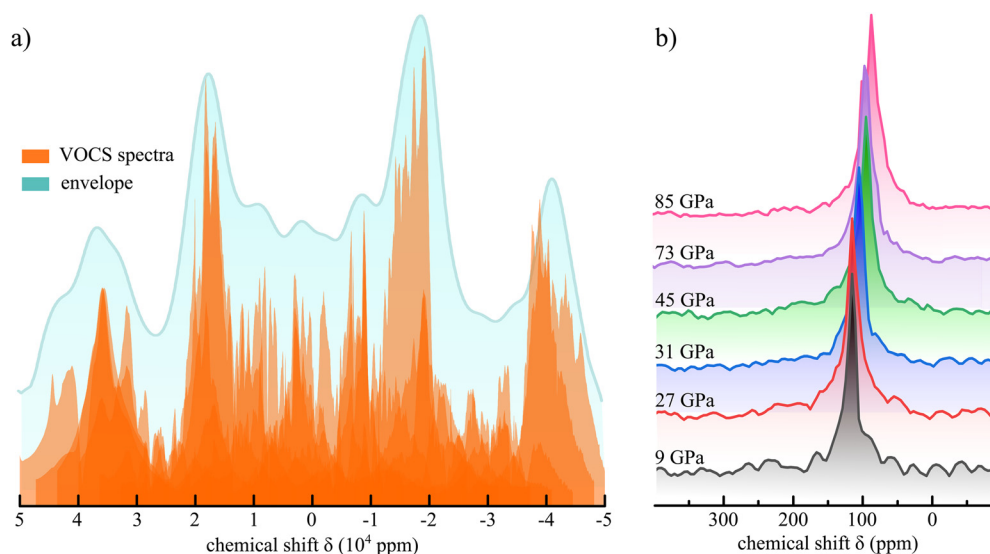


FIG. 4. ^{14}N -LG-NMR spectra of molecular nitrogen up to 85 GPa. (a) The quintuplet state of molecular nitrogen $^{14}\text{N}_2$ possesses a nuclear molecular spin $I = 2$, leading to significantly broadened spectra of about 2 MHz ($\approx 10^5$ ppm). The full spectrum is a sum of spin echoes (orange) acquired at variable frequency offsets. The blue spectrum is a broadened envelope of all subspectra. (b) Application of LG decoupling allowed the resolution of isotropic chemical shifts of molecular nitrogen at ultrahigh densities with an accuracy of ~ 10 ppm.

temperature displayed a 2 MHz broad ($\sim 10^5$ ppm) ^{14}N -NMR spectrum [see Fig. 4(a)]. The full spectrum was acquired using the well-established variable-offset cumulative spectroscopy (VOCS) method.³⁵

Figure 4(b) shows high-resolution spectra between 9 and 85 GPa. Considering a chemical shift dispersion range of ^{14}N of about 900 ppm,³⁶ spectral resolutions are sufficient to resolve individual chemical shifts of the ^{14}N spin system under pressure. A gradual shift of the signals toward lower ppm values was observed, which could indicate changes in the local environment of the ^{14}N nuclei. Details of our further analysis will be presented at a later stage.

B. Two dimensions

While one-dimensional LG-NMR experiments have proved to be a powerful tool to adequately resolve chemical shifts of homogeneous sample environments in DACs, signal detection in very heterogeneous systems or in systems with many different chemical environments or phases remains difficult.

To deal with strongly overlapping spectra of different local chemical environments in one phase or coexisting phases, a deconvolution in a second or even more dimensions is a well-established method in NMR spectroscopy.³⁷ In the case of LG-based homonuclear decoupling experiments, a second Fourier transform in the indirect LG time domain correlates both laboratory- and rotating-frame free induction decays and is therefore an obvious choice for a second dimension.

The advantage of using such 2D high-resolution NMR spectra compared with their 1D analog is that they allow parallel investigation of static line shapes in the F_1 projection, indicating, for example, proton mobility or coordination changes in quadrupolar nuclei via changes in the charge symmetry, and detection of isotropic chemical, Knight, or paramagnetic shifts in the F_2 projection. Three exemplary scenarios will be used to illustrate the usefulness of this multidimensional NMR technique in high-pressure research.

1. 2D-LG-NMR on ferromagnetic $\delta - (\text{Al}_{0.3}, \text{Fe}_{0.7})\text{OOH}$

Pure δ -AlOOH undergoes a subtle sub- to supergroup phase transition from the $\text{P2}_1\text{nm}$ to the Pnm phase at about 10 GPa^{38,39} and shows a hydrogen bond symmetrization at about 15 GPa.^{39–41} This oxyhydroxide has attracted attention in the geophysics community because of its potential role as a carrier of hydrogen into the deeper regions of the Earth's mantle.^{42–45} Iron incorporation (replacing Al atoms with Fe) is expected under mantle conditions and introduces a spin transition from a $S = 5/2$ high-spin state to a $S = 1/2$ low-spin state between 37 and 48 GPa,⁴⁴ and it may influence the structural phase transition, as well as the hydrogen bond symmetrization.

In Fig. 5(a), the local neighborhood of the O–H–O bond is visualized with a hydrogen atom at its center. Each oxygen is bound to three metal atoms, which are either Al^{3+} or Fe^{3+} cations, depending on the iron content. Assuming a stochastic distribution, six different hydrogen bond environments should be present. Figure 5(c) shows the theoretical probability distribution according to the stoichiometry of our $\delta - (\text{Al}_{0.3}, \text{Fe}_{0.7})\text{OOH}$ sample (the synthesis of the single crystal is described in detail in Ref. 38). The hydrogen bond species Q^i ($i = 1, \dots, 6$) denote the amount of ferric iron cations bound to the O–H–O subsystem.

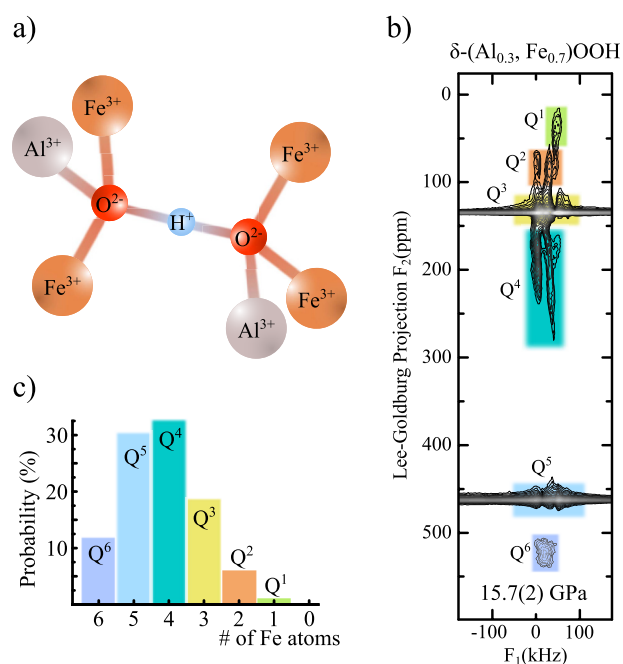


FIG. 5. High-resolution 2D-LG-NMR on ferromagnetic $(\text{Al}_{0.3}, \text{Fe}_{0.7})\text{OOH}$. (a) Local atomic structure of the hydrogen bond ensembles in $(\text{Al}_{0.3}, \text{Fe}_{0.7})\text{OOH}$. As both Al^{3+} and Fe^{3+} cations are statistically distributed, several hydrogen bond environments are likely to appear in the ^1H -NMR spectra. (b) 2D- ^1H LG-NMR spectrum at 15.7 GPa. The hydrogen-bonded species Q^i ($i = 1, \dots, 6$) appear at different paramagnetic shift values in the indirect LG projection dimension. Using the probability distribution of these species according to the stoichiometry of the sample (c), signal assignment via intensity ratios was possible.

Figure 5(b) shows a high-resolution 2D-LG ^1H -NMR spectrum of $\delta - (\text{Al}_{0.3}, \text{Fe}_{0.7})\text{OOH}$ at 15.7 GPa. Inspection of the area at $F_1 \approx 20$ kHz revealed a number of additional, formerly unresolvable signals. The 2D peak intensities of these additional signals were found to follow the probability distribution of the Q^i species, allowing for signal assignment in the 2D spectrum.

Since the isotropic part of the paramagnetic shielding tensor is proportional to the total electron spin number S and the local electron density of the paramagnetic centers at the NMR probe nucleus,⁴⁶ it is reasonable to assume that the resonance signals shift to higher ppm values with increasing amount of ferric iron in the close surrounding, starting with Fe^{3+} -depleted H-bond environments ($Q^{0,1}$) akin to pure δ -AlOOH and ending with fully Fe^{3+} -occupied coordination shells similar to ϵ -FeOOH. It is therefore possible to distinguish different local environments in the 2D-LG decomposition, enabling investigation of the individual behaviors of the spin subsystems as a function of local iron content. A more detailed analysis of the high-pressure behavior of these systems will be presented elsewhere.

2. Spin transition in dense magnesium silicate phase D

2D high-resolution signal detection in DACs can also be employed to observe otherwise undetectable electronic transitions. Figure 6 shows 2D-LG- ^1H -NMR spectra of dense magnesium silicate phase D [($\text{Mg}_{0.88}$,

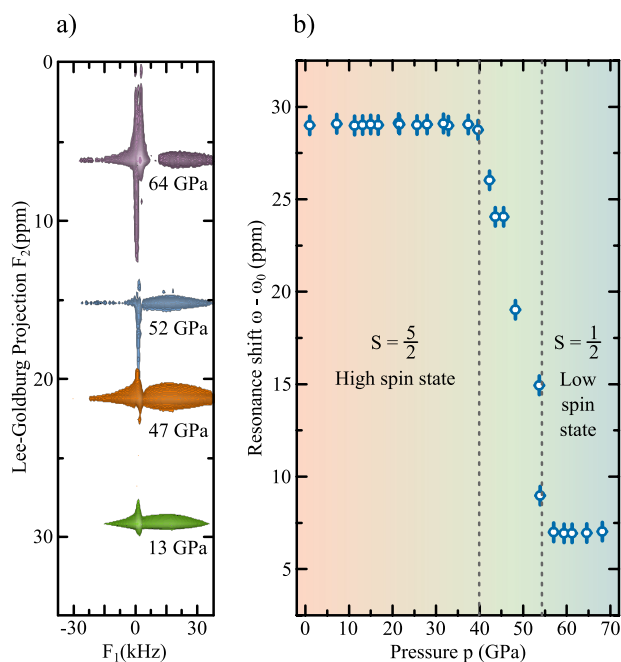


FIG. 6. 2D- ^1H -LG-NMR spectra of dense magnesium silicate phase D ($\text{Mg}_{0.88}\text{Fe}_{0.12}\cdot(\text{Si}_{0.9}\text{Al}_{0.1})_2\text{O}_6\text{H}_2$). (a) The spectra have linewidths in the LG projection dimension of less than 1 ppm, allowing the observation of the high-spin to low-spin transition of the ferric Fe^{3+} ions resulting in a partial collapse of the paramagnetic shift interaction with the hydrogen nuclei. (b) Resonance shift $\omega - \omega_0$ at pressures between 70 GPa and ambient conditions. Under the influence of strong paramagnetic interactions in the high-spin state below 40 GPa, the ^1H -NMR signals of phase D are shifted by 30 ppm downfield (higher ppm values). The electron spin crossover to a low-spin configuration leads to a pronounced reduction in the paramagnetic shift at higher pressures.

$\text{Fe}_{0.12}\cdot(\text{Si}_{0.9}\text{Al}_{0.1})_2\text{O}_6\text{H}_2$.⁴⁷ Because of the low concentration of iron in this sample, the high-spin to low-spin transition of ferric iron at $P \approx 43$ GPa is not observable by diffraction methods via a volume collapse of the FeO_6 octahedra. Also, the presence of both divalent and trivalent iron in these samples complicates Mössbauer spectroscopy owing to the greatly overlapping signals, hindering a straightforward observation of the electron spin collapse.

Contrastingly, ^1H -NMR signals of the hydrogen atoms in phase D were found to be well resolved in the indirect LG frequency domain, with linewidths of ~ 1 ppm. Furthermore, the presence of paramagnetic centers leads to a significant enhancement of spin-lattice relaxation times and thus allows rapid data acquisition.⁴⁶ The positions of the resonances shift toward lower ppm values, from initially about 30 ppm at 40 GPa to 6 ppm at higher pressures [Fig. 6(b)]. This transition was not observable using standard NMR excitation pulse sequences, since the resonance linewidths were found to be in excess of 200 ppm. Hydrogen signals stemming from paramagnetic interactions with high-spin divalent iron atoms ($S = 2$) were not observed within the chosen spectral range (≈ 300 ppm).

3. Phase heterogeneity in metal hydrides

One of the most intriguing discoveries in the past few years has been the observation of near-room-temperature superconductivity in metal

hydrides,⁴⁸ based on first-principles considerations.⁴⁹ Following the initial detection in H_3S at 204 K and $P \approx 150$ GPa,⁵⁰ it was rapidly realized that hydrogen incorporation into metallic parent lattices under high- P high- T conditions might be a route to a novel family of high-temperature superconductors.⁵¹ Recently, evidence for Cooper pair condensation has been found in clathrate-like superhydrides such as LaH_{10} ,^{52,53} as well as in carbonaceous sulfur hydrides.⁵⁴

However, sample synthesis and structure determination in DACs at the pressures (≥ 100 GPa) necessary for stabilization of these hydride structures are often challenging⁵⁵ and more or less limited to diffraction methods probing only the metal parent lattices or transport measurements.⁵⁶

NMR spectroscopy could yield information about the electronic and dynamic properties of the hydrogen subsystems in these compounds. Our first experiments on iron¹¹ and copper⁵⁷ hydrides demonstrated that NMR can be used to detect hydrogen systems associated with metallic metal hydride phases synthesized at high pressure under laser heating conditions and that in combination with density functional theory (DFT)-based electronic structure calculations, different coexisting hydrides can be distinguished by their electronic properties, if their signals do not strongly overlap.⁵⁷

However, laser-heated sample synthesis is prone to phase heterogeneity, in which multiple metastable phases, which are similar in their electronic structure, can be synthesized along the steep thermal gradient of laser focus spots,⁵⁶ which leads potentially to substantial signal overlap of static ^1H -NMR spectra. In this situation, 2D-LG-NMR can be used not only to resolve signals from hydride phases that vary only slightly in their hydrogen content, but also to detect low abundances of such phases, since the NMR signal intensity is in general proportional to the absolute abundance of each spin system or structure.

Figure 7 shows a high-resolution LG spectrum of yttrium hydrides synthesized from a mixture of yttrium powder and paraffin oil at 45 GPa under laser heating at up to 2500 K. Diffraction experiments suggest the predominant presence of two yttrium hydrides under

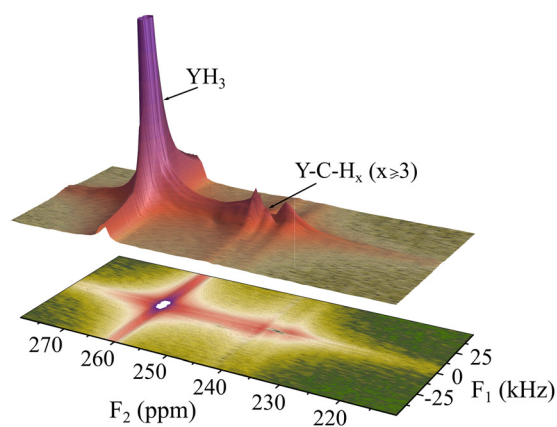


FIG. 7. High-resolution ^1H -NMR spectrum of yttrium hydrides synthesized at 45 GPa and 2500 K. The spectrum of YH_2 appears at 0 ppm and is not shown. In addition to synthesized YH_3 , the formation of at least one other hydride of slightly higher hydrogen content than YH_3 or of ternary compounds with incorporation of carbon can be observed.

these conditions: nonmetallic YH_2 and metallic YH_3 .^{58,59} The former will, in the absence of paramagnetic centers, be dominated by diamagnetic chemical shift interactions within $F_2 \leq 20$ ppm, while the latter, being metallic, will be under the strong influence of Pauli hyperfine interaction, leading to a pronounced Knight shift.

We find four peaks in the 2D spectrum: a peak at a shift of 0 ppm, a pronounced peak at 263 ppm, and at least two additional weak signals at slightly lower shifts (Fig. 7). We attribute the signal at 0 ppm to nonmetallic YH_2 . The additional signals may stem from metallic yttrium hydride phases, and consequently the spin–lattice relaxation times of these spin systems should follow the Korringa relation for Fermi-contact-driven electron–nuclear hyperfine interaction:

$$T_1 = \frac{\hbar}{4\pi k_B} \cdot \left(\frac{\gamma_e}{\gamma_n} \right)^2 \cdot \frac{1}{K_s^2 T}, \quad (6)$$

where γ_e and γ_n are the gyromagnetic ratios of the electron and the hydrogen nucleus, respectively, T is the sample temperature, and K_s is the Fermi contact term of the Knight shift. From Eq. (6), spin–lattice relaxation times T_1 of the order of 10 ms could be anticipated.

Using saturation recovery experiments, we found T_1 values of 8–12 ms, in excellent agreement with the theoretical Korringa relation, evidencing the metallic character of the observed signals (Fig. 7). Therefore, we attribute the signal at 263 ppm to YH_3 . The presence of weaker signals in addition to the expected signals of YH_2 and YH_3 in the high-resolution LG spectrum suggests the formation of either YH_x phases with slightly higher hydrogenation⁵⁷ or possible metallic ternary compounds formed by incorporation of carbon from the paraffin hydrogen reservoir or from the diamond anvils. Further investigation of the reaction dynamics as well as supporting DFT-based computations will hopefully help to identify these additional signals and will be presented at a later stage.

Nevertheless, this preliminary analysis of the data shows that it is possible to deconvolute NMR signals of several metal hydride phases simultaneously synthesized in one DAC. Therefore, the limitations that non-phase-pure synthesis imposes on other experimental techniques do not influence LG-NMR experiments in the same way, providing an opportunity to simultaneously investigate several coexisting metallic and possible superconducting phases under the same conditions of temperature and pressure.

VI. CONCLUSION

In this work, we have presented the first high-resolution high-pressure NMR experiments in DACs using the well-established method in which a rotating radio-frequency magnetic field aligned at the magic angle relative to the external magnetic field. We have shown that this method for resonance line narrowing is particularly suitable for our Lenz-lens-based high-pressure approach to NMR spectroscopy, leading to improvements in spectral resolution to 1 ppm and below. Several contemporary applications from the fields of condensed matter research, geophysics and solid-state physics,⁶⁰ and high-pressure chemistry⁶¹ demonstrate the wide applicability of this method.

Furthermore, there are a number of possible additional developments that have not been presented in this work, such as

- (i) further improvements in sensitivity for small sample fractions in the 2D spectra;
- (ii) combination of high-pressure NMR with structural search calculations, as suggested by Monserrat *et al.*;⁶²
- (iii) phase-sensitive measurements of superconducting properties.

These will hopefully lead to significantly more widespread use of NMR spectroscopy in high-pressure research and establish high-pressure NMR crystallography as an additional experimental tool complementing diffraction methods, in particular with regard to low- Z materials⁶³ and DFT-based calculations.⁶⁴

ACKNOWLEDGMENTS

We thank Nobuyoshi Miyajima for help with the FIB milling. We thank the German Research Foundation (Deutsche Forschungsgemeinschaft, DFG, Project Nos. DU 954/11-1, DU 393/13-1, DU 393/9-2, and ME 5206/3-1) and the Federal Ministry of Education and Research, Germany (BMBF, Grant No. 05K19WC1) for financial support. T.M. thanks the Center for High Pressure Science and Technology Advanced Research for financial support. F.T. thanks the Swedish Research Council (VR) (Grant No. 2019-05600). D.L. thanks the Alexander von Humboldt Foundation for financial support. N.D. thanks the Swedish Government Strategic Research Area in Materials Science on Functional Materials at Linköping University (Faculty Grant SFO-Mat-LiU No. 2009 00971).

AUTHOR DECLARATIONS

Conflict of Interest

The authors have no conflict of interests associated with the presented work.

DATA AVAILABILITY

The data supporting the findings of this study are publicly available from the corresponding author upon reasonable request.

REFERENCES

- ¹M. Levitt, *Spin Dynamics: Basics of Nuclear Magnetic Resonance*, 2nd ed., Concepts in Magnetic Resonance Part A (John Wiley & Sons, Ltd., 2009), Vol.34A, pp. 60–61.
- ²D. M. Grant and K. H. Robin, in *Encyclopedia of Magnetic Resonance*, 1st ed., edited by K. H. Grant and D. M. Robin (Wiley-VCH Verlag, 2007).
- ³N. Dubrovinskaia and L. Dubrovinsky, “Crystallography taken to the extreme,” *Phys. Scr.* **93**, 062501 (2018).
- ⁴M. W. MacArthur, P. C. Driscoll, and J. M. Thornton, “NMR and crystallography—Complementary approaches to structure determination,” *Trends Biotechnol.* **12**, 149–153 (1994).
- ⁵D. L. Bryce, “NMR crystallography: Structure and properties of materials from solid-state nuclear magnetic resonance observables,” *IUCrJ* **4**, 350–359 (2017).
- ⁶C. Martineau, “NMR crystallography: Applications to inorganic materials,” *Solid State Nucl. Magn. Reson.* **63–64**, 1–12 (2014).
- ⁷H.-K. Mao, B. Chen, J. Chen, K. Li, J.-F. Lin, W. Yang, and H. Zheng, “Recent advances in high-pressure science and technology,” *Matter Radiat. Extremes* **1**, 59–75 (2016).
- ⁸T. Meier, “At its extremes: NMR at giga-pascal pressures,” in *Annual Reports on NMR Spectroscopy*, 93rd ed., edited by G. Webb (Elsevier, London, 2018), Chap. 1, pp. 1–74.
- ⁹T. Meier, N. Wang, D. Mager, J. G. Korvink, S. Petitgirard, and L. Dubrovinsky, “Magnetic flux tailoring through Lenz lenses for ultrasmall samples: A new pathway

- to high-pressure nuclear magnetic resonance,” *Sci. Adv.* **3**, eaao5242 (2017); [arXiv:1706.00073](https://arxiv.org/abs/1706.00073).
- ¹⁰T. Meier, S. Khandarkhaeva, S. Petitgirard, T. Körber, A. Lauener, E. Rössler, and L. Dubrovinsky, “NMR at pressures up to 90 GPa,” *J. Magn. Reson.* **292**, 44–47 (2018); [arXiv:1803.05472](https://arxiv.org/abs/1803.05472).
- ¹¹T. Meier, F. Trybel, S. Khandarkhaeva, G. Steinle-Neumann, S. Chariton, T. Fedotenko, S. Petitgirard, M. Hanfland, K. Glazyrin, N. Dubrovinskaia, and L. Dubrovinsky, “Pressure-induced hydrogen-hydrogen interaction in metallic FeH revealed by NMR,” *Phys. Rev. X* **9**, 031008 (2019); [arXiv:1902.03182](https://arxiv.org/abs/1902.03182).
- ¹²T. Meier, A. P. Dwivedi, S. Khandarkhaeva, T. Fedotenko, N. Dubrovinskaia, and L. Dubrovinsky, “Table-top nuclear magnetic resonance system for high-pressure studies with *in situ* laser heating,” *Rev. Sci. Instrum.* **90**, 123901 (2019); [arXiv:1909.09406](https://arxiv.org/abs/1909.09406).
- ¹³T. Meier, “Journey to the centre of the Earth: Jules Verne’s dream in the laboratory from an NMR perspective,” *Prog. Nucl. Magn. Reson. Spectrosc.* **106–107**, 26–36 (2018); [arXiv:1803.04643](https://arxiv.org/abs/1803.04643).
- ¹⁴S. A. Smith, W. E. Palke, and J. T. Gerig, “The Hamiltonians of NMR. Part I,” *Concepts Magn. Reson.* **4**, 107–144 (1992).
- ¹⁵G. E. Pake, “Nuclear resonance absorption in hydrated crystals: Fine structure of the proton line,” *J. Chem. Phys.* **16**, 327–336 (1948).
- ¹⁶J. W. Hennel and J. Klinowski, “Magic-angle spinning: A historical perspective,” in *New Techniques in Solid-State NMR*, 246th ed., Topics in Current Chemistry Vol. 2, edited by J. Klinowski (Springer, Berlin, Heidelberg, 2005), pp. 1–14.
- ¹⁷T. Meier, T. Herzog, and J. Haase, “Moissanite anvil cell design for giga-pascal nuclear magnetic resonance,” *Rev. Sci. Instrum.* **85**, 043903 (2014).
- ¹⁸T. Meier, S. Petitgirard, S. Khandarkhaeva, and L. Dubrovinsky, “Observation of nuclear quantum effects and hydrogen bond symmetrisation in high pressure ice,” *Nat. Commun.* **9**, 2766 (2018); [arXiv:1803.07019](https://arxiv.org/abs/1803.07019).
- ¹⁹T. Meier, D. Laniel, M. Pena-Alvarez, F. Trybel, S. Khandarkhaeva, A. Krupp, J. Jacobs, N. Dubrovinskaia, and L. Dubrovinsky, “Nuclear spin coupling crossover in dense molecular hydrogen,” *Nat. Commun.* **11**, 6334 (2020).
- ²⁰M. Lee and W. I. Goldberg, “Nuclear-magnetic-resonance line narrowing by a rotating rf field,” *Phys. Rev.* **140**, A1261–A1271 (1965).
- ²¹T. Meier, S. Reichardt, and J. Haase, “High-sensitivity NMR beyond 200 000 atmospheres of pressure,” *J. Magn. Reson.* **257**, 39–44 (2015).
- ²²T. Meier, S. Khandarkhaeva, J. Jacobs, N. Dubrovinskaia, and L. Dubrovinsky, “Improving resolution of solid state NMR in dense molecular hydrogen,” *Appl. Phys. Lett.* **115**, 131903 (2019); [arXiv:1908.01150v1](https://arxiv.org/abs/1908.01150v1).
- ²³Y. Akahama and H. Kawamura, “High-pressure Raman spectroscopy of diamond anvils to 250 GPa: Method for pressure determination in the multimegabar pressure range,” *J. Appl. Phys.* **96**, 3748 (2004).
- ²⁴Y. Akahama and H. Kawamura, “Pressure calibration of diamond anvil Raman gauge to 310GPa,” *J. Appl. Phys.* **100**, 043516 (2006).
- ²⁵R. R. Ernst, G. Bodenhausen, A. Wokaun, and A. G. Redfield, “Principles of nuclear magnetic resonance in one and two dimensions,” *Phys. Today* **42**(7), 75–76 (1989).
- ²⁶E. Gregoryanz, C. Ji, P. Dalladay-Simpson, B. Li, R. T. Howie, and H.-K. Mao, “Everything you always wanted to know about metallic hydrogen but were afraid to ask,” *Matter Radiat. Extremes* **5**, 038101 (2020).
- ²⁷R. P. Dias and I. F. Silvera, “Observation of the Wigner-Huntington transition to metallic hydrogen,” *Science* **355**, 715–718 (2017); [arXiv:1610.01634](https://arxiv.org/abs/1610.01634).
- ²⁸H. Y. Geng, “Public debate on metallic hydrogen to boost high pressure research,” *Matter Radiat. Extremes* **2**, 275–277 (2017).
- ²⁹D. Laniel, B. Winkler, T. Fedotenko, A. Pakhomova, S. Chariton, V. Milman, V. Prakapenka, L. Dubrovinsky, and N. Dubrovinskaia, “High-pressure polymeric nitrogen allotrope with the black phosphorus structure,” *Phys. Rev. Lett.* **124**, 216001 (2020); [arXiv:2003.02758](https://arxiv.org/abs/2003.02758).
- ³⁰Y. Li, X. Feng, H. Liu, J. Hao, S. A. T. Redfern, W. Lei, D. Liu, and Y. Ma, “Route to high-energy density polymeric nitrogen *t*-N via He–N compounds,” *Nat. Commun.* **9**, 722 (2018).
- ³¹D. Laniel, B. Winkler, E. Koemets, T. Fedotenko, M. Bykov, E. Bykova, L. Dubrovinsky, and N. Dubrovinskaia, “Synthesis of magnesium-nitrogen salts of polynitrogen anions,” *Nat. Commun.* **10**, 4515 (2019).
- ³²D. Laniel, G. Weck, and P. Loubeyre, “Direct reaction of nitrogen and lithium up to 75 GPa: Synthesis of the Li₃N, LiN, LiN₂, and LiN₅ compounds,” *Inorg. Chem.* **57**, 10685–10693 (2018).
- ³³D. Laniel, G. Weck, G. Gaiffe, G. Garbarino, and P. Loubeyre, “High-pressure synthesized lithium pentazolate compound metastable under ambient conditions,” *J. Phys. Chem. Lett.* **9**, 1600–1604 (2018).
- ³⁴L. A. O’Dell and C. I. Ratcliffe, “Ultra-wideline ¹⁴N NMR spectroscopy as a probe of molecular dynamics,” *Chem. Commun.* **46**, 6774–6776 (2010).
- ³⁵R. W. Schurko, “Ultra-wideline solid-state NMR spectroscopy,” *Acc. Chem. Res.* **46**, 1985–1995 (2013).
- ³⁶M. Witanowski, L. Stefaniak, and G. A. Webb, “Nitrogen NMR spectroscopy,” in *Annual Reports on NMR Spectroscopy*, edited by G. Webb (Elsevier, 1993), Vol. 25, pp. 1–82.
- ³⁷R. S. Macomber and G. S. Harbison, “A complete introduction to modern NMR spectroscopy,” *Phys. Today* **52**(1), 68 (1999).
- ³⁸D. Simonova, E. Bykova, M. Bykov, T. Kawazoe, A. Simonov, N. Dubrovinskaia, and L. Dubrovinsky, “Structural study of δ -AlOOH up to 29 GPa,” *Minerals* **10**, 1055 (2020).
- ³⁹A. Sano-Furukawa, T. Hattori, K. Komatsu, H. Kagi, T. Nagai, J. J. Molaison, A. M. dos Santos, and C. A. Tulk, “Direct observation of symmetrization of hydrogen bond in δ -AlOOH under mantle conditions using neutron diffraction,” *Sci. Rep.* **8**, 15520 (2018).
- ⁴⁰S. B. Pillai, P. K. Jha, A. Padmalal, D. M. Maurya, and L. S. Chamyal, “First principles study of hydrogen bond symmetrization in δ -AlOOH,” *J. Appl. Phys.* **123**, 115901 (2018).
- ⁴¹P. Cortona, “Hydrogen bond symmetrization and elastic constants under pressure of δ -AlOOH,” *J. Phys.: Condens. Matter* **29**, 325505 (2017).
- ⁴²A. Sano, E. Ohtani, T. Kondo, N. Hirao, T. Sakai, N. Sata, Y. Ohishi, and T. Kikegawa, “Aluminous hydrous mineral δ -AlOOH as a carrier of hydrogen into the core-mantle boundary,” *Geophys. Res. Lett.* **35**, L03303, <https://doi.org/10.1029/2007gl031718> (2008).
- ⁴³Y. Duan, N. Sun, S. Wang, X. Li, X. Guo, H. Ni, V. B. Prakapenka, and Z. Mao, “Phase stability and thermal equation of state of δ -AlOOH: Implication for water transportation to the deep lower mantle,” *Earth Planet. Sci. Lett.* **494**, 92–98 (2018).
- ⁴⁴X. Su, C. Zhao, C. Lv, Y. Zhuang, N. Salke, L. Xu, H. Tang, H. Gou, X. Yu, Q. Sun *et al.*, “The effect of iron on the sound velocities of δ -AlOOH up to 135 GPa,” *Geosci. Front.* **12**, 937–946 (2021).
- ⁴⁵H.-k. Mao and W. L. Mao, “Key problems of the four-dimensional Earth system,” *Matter Radiat. Extremes* **5**, 038102 (2020).
- ⁴⁶A. J. Pell, G. Pintacuda, and C. P. Grey, “Paramagnetic NMR in solution and the solid state,” *Prog. Nucl. Magn. Reson. Spectrosc.* **111**, 1–271 (2019).
- ⁴⁷H. Yuan and L. Zhang, “In situ determination of crystal structure and chemistry of minerals at Earth’s deep lower mantle conditions,” *Matter Radiat. Extremes* **2**, 117–128 (2017).
- ⁴⁸X.-J. Chen, “Exploring high-temperature superconductivity in hard matter close to structural instability,” *Matter Radiat. Extremes* **5**, 068102 (2020).
- ⁴⁹N. W. Ashcroft, “Hydrogen dominant metallic alloys: High temperature superconductors?,” *Phys. Rev. Lett.* **92**, 187002 (2004).
- ⁵⁰A. P. Drozdov, M. I. Erements, I. A. Troyan, V. Ksenofontov, and S. I. Shylin, “Conventional superconductivity at 203 kelvin at high pressures in the sulfur hydride system,” *Nature* **525**, 73–76 (2015).
- ⁵¹J. Lv, Y. Sun, H. Liu, and Y. Ma, “Theory-orientated discovery of high-temperature superconductors in superhydrides stabilized under high pressure,” *Matter Radiat. Extremes* **5**, 068101 (2020).
- ⁵²A. P. Drozdov, P. P. Kong, V. S. Minkov, S. P. Besedin, M. A. Kuzovnikov, S. Mozaffari, L. Balicas, F. F. Balakirev, D. E. Graf, V. B. Prakapenka, E. Greenberg, D. A. Knyazev, M. Tkacz, and M. I. Erements, “Superconductivity at 250 K in lanthanum hydride under high pressures,” *Nature* **569**, 528–531 (2019).
- ⁵³M. Somayazulu, M. Ahart, A. K. Mishra, Z. M. Geballe, M. Baldini, Y. Meng, V. V. Struzhkin, and R. J. Hemley, “Evidence for superconductivity above 260 K in lanthanum superhydride at megabar pressures,” *Phys. Rev. Lett.* **122**, 027001 (2019); [arXiv:1808.07695](https://arxiv.org/abs/1808.07695).
- ⁵⁴E. Snider, N. Dasenbrock-Gammon, R. McBride, M. Debessai, H. Vindana, K. Vencatasamy, K. V. Lawler, A. Salamat, and R. P. Dias, “Room-temperature superconductivity in a carbonaceous sulfur hydride,” *Nature* **586**, 373–377 (2020).

- ⁵⁵V. Struzhkin, B. Li, C. Ji, X.-J. Chen, V. Prakapenka, E. Greenberg, I. Troyan, A. Gavriluk, and H.-k. Mao, "Superconductivity in La and Y hydrides: Remaining questions to experiment and theory," *Matter Radiat. Extremes* **5**, 028201 (2020).
- ⁵⁶P. P. Kong, V. S. Minkov, M. A. Kuzovnikov, S. P. Besedin, A. P. Drozdov, S. Mozaffari, *et al.* "Superconductivity up to 243 K in yttrium hydrides under high pressure" (unpublished) (2019).
- ⁵⁷T. Meier, F. Trybel, G. Criniti, D. Laniel, S. Khandarkhaeva, E. Koemets, T. Fedotenko, K. Glazyrin, M. Hanfland, M. Bykov, G. Steinle-Neumann, N. Dubrovinskaia, and L. Dubrovinsky, "Proton mobility in metallic copper hydride from high-pressure nuclear magnetic resonance," *Phys. Rev. B* **102**, 165109 (2020).
- ⁵⁸Y. Li, J. Hao, H. Liu, J. S. Tse, Y. Wang, and Y. Ma, "Pressure-stabilized superconductive yttrium hydrides," *Sci. Rep.* **5**, 9948 (2015).
- ⁵⁹L. L. Liu, H. J. Sun, C. Z. Wang, and W. C. Lu, "High-pressure structures of yttrium hydrides," *J. Phys.: Condens. Matter* **29**, 325401 (2017).
- ⁶⁰H.-K. Mao, B. Chen, H. Gou, K. Li, J. Liu, L. Wang, H. Xiao, and W. Yang, "2020—Transformative science in the pressure dimension," *Matter Radiat. Extremes* **6**, 013001 (2021).
- ⁶¹C.-S. Yoo, "Chemistry under extreme conditions: Pressure evolution of chemical bonding and structure in dense solids," *Matter Radiat. Extremes* **5**, 018202 (2020).
- ⁶²B. Monserrat, S. E. Ashbrook, and C. J. Pickard, "Nuclear magnetic resonance spectroscopy as a dynamical structural probe of hydrogen under high pressure," *Phys. Rev. Lett.* **122**, 135501 (2019); [arXiv:1902.10721](https://arxiv.org/abs/1902.10721).
- ⁶³C. Ji, B. Li, W. Liu, J. S. Smith, A. Björling, A. Majumdar, W. Luo, R. Ahuja, J. Shu, J. Wang, S. Sinogeikin, Y. Meng, V. B. Prakapenka, E. Greenberg, R. Xu, X. Huang, Y. Ding, A. Soldatov, W. Yang, G. Shen, W. L. Mao, and H.-K. Mao, "Crystallography of low Z material at ultrahigh pressure: Case study on solid hydrogen," *Matter Radiat. Extremes* **5**, 038401 (2020).
- ⁶⁴D. V. Semenov, I. A. Kruglov, I. A. Savkin, A. G. Kvashnin, and A. R. Oganov, "On distribution of superconductivity in metal hydrides," *Curr. Opin. Solid State Mater. Sci* **24** (2), 100808 (2020).